Title
Anillin, a contractile ring protein that cycles from the nucleus to the cell cortex.

Permalink
https://escholarship.org/uc/item/7kx1676f

Journal
Journal of Cell Biology, 131(1)

ISSN
0021-9525

Authors
Field, CM
Alberts, BM

Publication Date
1995-10-01

DOI
10.1083/jcb.131.1.165

Peer reviewed

Anillin, a Contractile Ring Protein That Cycles from the Nucleus to the Cell Cortex

Christine M. Field and Bruce M. Alberts

Department of Biochemistry and Biophysics, University of California at San Fancisco Medical Center, San Francisco, California 94143-0448

Abstract. We report the cDNA sequence and localization of a protein first identified by actin filament chromatography of *Drosophila* embryo extracts as ABP8 (Miller, K. G., C. M. Field, and B. M. Alberts. 1989. *J. Cell Biol.* 109:2963–2975). The cDNA encodes a 1201–amino acid protein which we name anillin. Anillin migrates at 190 kD on SDS-PAGE. Anillin is expressed throughout *Drosophila* development and in tissue culture cells. By immunofluorescence, anillin localizes to the nucleus of interphase cells, except in the syncytial embryo where it is always cytoplasmic. During metaphase, it is present in the cytoplasm and cortex, and during anaphase–telophase it becomes highly enriched in the cleavage furrow along with myosin II. In the syncytial embryo, anillin, along with myosin-II, is enriched in cortical areas undergoing cell cycle regulated invagination including metaphase furrows and the cellularization front. In contractile rings, metaphase furrows, and nascent ring canals, anillin remains bound to the invaginated cortex suggesting a stabilizing role. Anillin is not expressed in cells that have left the cell cycle. Anillin isolated from embryo extracts binds directly to actin filaments. The domain responsible for this binding has been mapped to a region of 244 amino acids by expression of protein fragments in bacteria. This domain, which is monomeric in solution, also bundles actin filaments. We speculate that anillin plays a role in organizing and/or stabilizing the cleavage furrow and other cell cycle regulated, contractile domains of the actin cytoskeleton.

C
YTOKINESIS is thought to be driven by a contractile ring of actin and myosin which determines the plane of cleavage and generates the force that pinches off the membrane between daughter cells (Salmon, 1989; Satterwhite and Pollard, 1992; Sanders and Field, 1994). The orientation of this ring is governed by the positions of the mitotic spindle through an unknown mechanism (Rappaport and Rappaport, 1974). During late anaphase, the cell cortex changes in the region where the cleavage furrow will form. Both myosin II and the recently identified septin protein, peanut (Neufeld and Rubin, 1994), concentrate in a band around the cell equator forming a contractile ring. Actin filaments may also concentrate in the ring, although in many cell types this does not occur. Many questions remain to be answered about this process, including the identity of the other proteins required for assembly of the contractile ring and how its formation is regulated.

The *Drosophila* embryo provides a model system for studying cytokinesis. In addition to the normal cytokinesis observed during somatic cell divisions, the early embryo

exhibits other actin mediated cortical events that are mechanistically related to cytokinesis; including metaphase furrow formation and cellularization. The first 14 nuclear division cycles in *Drosophila* embryos occur in a syncytium. The nuclei are originally located in interior of the egg and during nuclear cycles 8–10, they migrate to the surface and form a monolayer just below the plasma membrane. In the ensuing syncytial blastoderm (nuclear cycles 10–14), the nuclei divide four times at the cortex without concomitant cytokinesis. During this period, the plasma membrane undergoes a series of movements and rearrangements that are cell cycle dependent. During interphase, cytoplasmic buds appear on the embryo surface. These buds collapse as the nucleus enters mitosis and the plasma membrane invaginates around each mitotic spindle forming a transient metaphase furrow. These furrows are thought to be required for the separation of neighboring mitotic spindles (Postner et. al., 1992; Sullivan et al., 1993) The actin cytoskeleton is required for both of these events. It alternately forms a cap over the nucleus during interphase and helps to shape the plasma membrane during metaphase furrow formation (reviewed in Schejter and Wieschaus, 1993).

During interphase of nuclear cycle 14, simultaneous membrane invaginations occur that enclose all the nuclei at the cortex and result in the formation of approximately 6,000 individual cells. The first stage of cellularization re-

---

sembles metaphase furrow formation, as the plasma membrane invaginates down around each nucleus. The final stage consists of a contraction at the base of the invagination that results in the pinching off of individual cells though these remain attached to the yolk center by thin necks until gastrulation movements occur (Warn and Robert-Nicoud, 1990). Cross-sections at the base of the invaginating furrow resemble contractile rings in that they are enriched in myosin II (Young et al., 1991) and peanut (Neufeld and Rubin, 1994). After cellularization, cells divide by forming normal cleavage furrows with groups of neighboring cells entering mitosis together in mitotic domains (Foe, 1989). The role of the actin cytoskeleton during *Drosophila* embryogenesis has been reviewed by Foe et al. (1993) and by Schejter and Wieschaus (1993).

In the early *Drosophila* embryo, maternally expressed genes have been identified that effect metaphase furrow formation (Postner et al., 1992; Sullivan et al., 1993). Similarly, three zygotic genes have been identified that specifically effect cellularization. These genes encode three novel proteins involved in stabilizing the hexagonal actin filament array (Rose and Wieschaus, 1992; Schejter and Wieschaus, 1993a; Schweisguth et al., 1990). A third type of mutation, pebble, allows metaphase furrow formation and cellularization to proceed correctly, while causing the subsequent process of cytokinesis to be defective (Hime and Saint, 1992; Lehner, 1992). The possiblity that a maternal contribution allows the furrow events prior to the first cell division to occur in the pebble mutant has not been ruled out.

Despite the differences identified by mutant analysis, processes of metaphase furrow formation, cellularization, and cytokinesis in *Drosophila* embryos are likely to share numerous protein components including components of the actin cytoskeleton. To identify such proteins, we have used actin filament affinity chromatography and immunofluorescence (Miller et al., 1989), focusing on a class of actin binding proteins that localize to metaphase furrows and to invaginating membranes during cellularization. In this report, we characterize the 190-kD protein recognized by antibody No. 8 in Miller et al. (1989) which is highly enriched at the tips of invaginating membrane furrows. We have named this novel protein *anillin* (from the Spanish *anillo*, for ring), in recognition of its ring-shaped distribution in dividing cells, where it is part of the cleavage furrow.

Materials and Methods

Actin Filament Column Construction and Isolation of Actin-associated Proteins

Actin columns, albumin control columns, embryo extracts, and chromatography conditions were described previously (Miller et al., 1989, 1991). Columns were loaded and washed in A buffer (50 mM TrisCl, pH 7.7, 0.5 mM Na₃ EDTA, 0.5 mM Na₃ EGTA, 1 mM DTT, 10% glycerol, 10 μg/ml each of leupeptin, pepstatin, and aprotinin), and then eluted stepwise with A buffer containing 0.5 M KCl followed by A buffer containing 1 M KCl, 1 mM ATP, 2 mM MgCl₂.

Cloning of Anillin

The first anillin cDNA clones were isolated from a Lambda Zap expression library (Hay et al., 1988) constructed from *Drosophila* ovary poly A+ RNA. It was screened as described (Huynh et al., 1985) with minor modi-

fications. This screen produced two related clones of 1.4 and 2.5 kb. The larger of the two was radioactively labeled using a random priming kit from GIBCO BRL (Gaithersburg, MD) as per manufacturer's instructions and used to screen a second cDNA library. The second library was made from 0–3 h embryos in lambda *gt-10* (Poole et al., 1985). We screened 450,000 plaques and isolated three related positive cDNAs. The combined sequences resulted in a cDNA of 3.9 kb. This sequence contained a start codon with a good upstream start consensus. (The four nucleotides upstream of the ATG start have a three out of four match to the consensus sequence found upstream of ATG's used as initiation codons in *Drosophila*. The C in position −2 is seen in 25% of the cases examined (Cavener, 1987)).

Northern blot analysis was used to determine the size of the anillin mRNA in RNA isolated from 0–2 h embryos. Because of the discrepancy in size between the cloned cDNA (3.9 kb) and the estimated size of the mRNA (slightly less than 4.3 kb) and the lack of inframe stop codons, we were concerned that the missing 400 bp might contain coding sequence.

We used a nested PCR approach to clone the missing cDNA (Gibbons, 1991) from a plasmid cDNA library (Brown, 1988). Two primers complementary to the cloning vector used for construction of the cDNA library and four primers taken from the 5′ end of the existing cDNA were used. These primers were used in pairs such that the first and longest reaction was carried out using the library as a template and then used as a seed for a subsequent reactions. PCR was performed using Taq polymerase and several different reactions were cloned and sequenced because of possible fidelity problems.

DNA Sequencing

DNA sequencing was performed by a primer walking strategy, using fluorescently labeled chain terminator nucleotides with an Applied Biosystems 373 automated sequencing machine (Biomolecular Resource Center, University of California, San Francisco, CA). Both strands were completely sequenced using overlapping primers so that each position could be confirmed from at least three separate reactions. The order of nonoverlapping cDNA fragments was determined by using the PCR with Taq polymerase (Boehringer-Mannheim Biochemicals, Indianapolis, IN) using standard conditions (Sambrook et al., 1989), and a genomic library (Brown and Kafatos, 1988) as a template.

Developmental Western Blot

Eggs were collected at two hour intervals at 22°C and then shifted to 25°C. To examine possible protein modifications, clarified extracts were used. Extracts were prepared as previously described (Miller et., al., 1989). Dechorionated embryos were diluted 1/10 with extract buffer; 5 mM Tris, pH 7.6, 0.5 mM EDTA, 0.5 mM EGTA, 0.05% NP-40 (Sigma Chemical Co., St. Louis, MO) plus protease inhibitors. The extract was spun at 10,000 g for 20′ and passed through cheesecloth to remove lipid. Equal amounts of protein were loaded per lane.

Expression and Purification of Fusion Proteins

We have used two types of fusion proteins in the experiments described here: a glutathione S-transferase (GST)[1] fusion protein, made using the pGEX expression vector (Smith, 1988), and 6xHis Affinity Tag proteins using the QIAexpress pQE vectors (Janknecht et al., 1991) from Quigen (Chatsworth, CA). For the 6xHis Tag proteins, PCR was used to generate the appropriate restriction fragments, using standard techniques (Sambrook et al., 1989) with Vent DNA polymerase from NEB (Beverly, MA). The 6xHis fragments were cloned into the vector PQE9 using a HindIII site and a SalI site. Therefore, they contained the amino acids MRGSGSVD in addition to the 6xhistidine tag. Vectors were transformed into either competent DH5 cells (GST fusion) or M15 (pREP4) cells (6xHis), and these cells were used to produce the desired fusion proteins as per the manufacturer's instructions. The GST and 6xHis fusion proteins were purified on glutathione-affinity columns and Ni-NTA resin columns, respectively. The 6xHis fusion proteins were often further characterized and purified with a Pharmacia FPLC system using a Superose 12 gel filtration column.

All fusion proteins used in this study are referred to by their amino acid

---

1. *Abbreviations used in this paper:* GST, glutathione s-transferase; NLS, nuclear localization sequence.

numbers. When constructing the anillin fragments for domain analysis, the clones used to express fragments 127-340, 127-318, and 204-371 were sequenced at both ends to confirm their position within the protein.

Immunological Methods

The original antibody used to screen the expression library was generated in two mice by immunizing with a doublet 190-kD SDS-PAGE gel band (Miller et al., 1989). Rabbit antibodies were generated by immunizing rabbits with purified GST-anillin 401-828 and 6xHis-anillin 1-371 (Berkeley Antibody Company, Richmond, CA).

Antibodies were affinity purified by passage over columns of immobilized fusion proteins. The GST-anillin 401-828 serum was first depleted of anti-GST antibodies by repeated passage over an Affigel 10 resin (Bio-Rad Laboratories, Richmond, CA) containing the GST protein. When no anti-GST antibodies remained, the serum was passed over a column containing GST-anillin 401-828. The 6xHis-anillin 1-371 antibody was affinity purified by passing serum over a column containing the appropriate 6xHis fusion protein. Protein columns were constructed by coupling the appropriate fusion protein in 50 mM Hepes, pH 7.6, 50 mM KCl or PBS (140 mM Na$_2$HPO$_4$, 1.8 mM KH$_2$PO$_4$, pH 7.2, 138 mM NaCl, 2.7 mM KCl) to an Affigel 10 resin at 3–10 mg of protein per ml of resin as per manufacturer's instructions.

After the serum was loaded over the column, the column was washed extensively with PBS or the Hepes buffer plus 0.5 M NaCl and the antibodies were then eluted with either 0.1 M glycine, pH 2.1, or 0.1 M Triethylamine, pH 11.0. The antibody solution was neutralized with an appropriate Tris buffer and dialyzed into either PBS or 5 mM potassium phosphate, 50 mM KCl, pH 7.2.

Western blotting was performed as described (Kellogg et al., 1989), using mouse antibodies diluted 1/500 or affinity-purified rabbit antibodies at 1–2 μg/ml, with alkaline phosphatase-labeled secondary antibody.

For immunofluorescence experiments, affinity-purified anti-GST-anillin 401-828 was directly labeled with tetramethyl-rhodamine-NHS ester (Molecular Probes, Eugene, OR) according to the manufacturer's directions.

Fixation and Immunofluorescence

Two fixatives were used for *Drosophila* embryos. Usually, embryos were fixed in 16.5% formaldehyde as described by (Theurkauf, 1992). Vitelline membranes were manually removed. For myosin II localization, embryos were fixed using a short heat treatment followed by methanol (Miller et al., 1989; Thomas and Kiehart, 1994). Embryos were stained with rhodamine-anti-GST-anillin 401-828 at 0.1–1 μg/ml, and in some cases also with FITC phalloidin at 0.1 μM (Sigma Chemical Co.). After washing, embryos were stained for 10 min with DAPI (Sigma Chemical Co.) at 2 μg/ml to label the DNA and were mounted in 90% glycerol, 20 mM Tris Cl, pH 8.0, 0.1% phenylenediamine.

Ovarioles were fixed and stained as described (Theurkauf et al., 1992). *Drosophila* tissue culture cells were cultured at 25°C in D22 insect medium (Sigma Chemical Co.). 10% fetal calf serum was added to the media when culturing Schneider cells. Cells were washed in PBS, fixed for 5 min in 3% formaldehyde and 0.1% glutaraldehyde in PBS, and permeabilized and blocked for 5 min in 0.1% Triton X-100, 2% albumin in PBS. They were stained and mounted as above.

Actin Cosedimentation Assay (Endogenous Anillin)

Endogenous anillin was isolated using immunoprecipitation. Anti-anillin and control (random rabbit IgG) antibodies were bound to protein A agarose beads (GIBCO BRL). Approximately 10–15 μg of anillin antibody was added to 100 μl of beads previously equilibrated in IP buffer (20 mM Tris, pH 7.6, 150 mM NaCl, 250 mM sucrose, 0.5 mM EDTA, 0.5 mM EGTA.) Both GST anillin 401-828 and 6xHis anillin 1-371 antibodies were tested. (See Fig. 10 for antibody locations.) Approximately 15 μg of random rabbit IgG was added to 100 μl of beads as a control. The antibody bead mixture was agitated gently at 4°C for ~1.5 h and then washed several times with IP buffer. Anillin was bound by adding various volumes of a clarified extract described previously (Miller et al., 1989.) The beads now bound with anillin were washed several times with IP buffer. Actin filaments stabilized with 10 μg/ml of phalloidin (Sigma Chemical Co.) were added to the beads to a final actin concentration of 10 μM and incubated at RT for 20 min with an additional 10-min incubation at 4°C. The

beads were sedimented through a step gradient consisting of 600 μl of 30% sucrose, 350 μl 60% sucrose in IP buffer for 4 min at 1,000 g. Proteins pelleted with the beads were fractionated by SDS-PAGE.

Actin Cosedimentation Assay (Bacterially Expressed Fragments)

The 6xHis tagged proteins eluted from the Ni-NTA columns at 1–5 mg/ml. They were dialyzed into PB (50 mM Tris Cl, pH 7.7, 20 mM KCl, 2 mM MgCl$_2$, 0.2 mM ATP) plus 1 mM DTT and 10% glycerol. Prior to mixing with phalloidin-stabilized actin filaments, fusion proteins were clarified by sedimentation at 100,000 g for 10 min. Immediately after spin, fusion proteins and actin filaments were diluted to 100 μl with PB containing 10 μM phalloidin and incubated for 15 min at 25°C with occasional agitation. The final concentration of actin was 20 μM. The final concentration of the fusion proteins ranged from 15–100 μM. The samples were then layered over 100 μl of PB containing 40% glycerol and sedimented at 100,000 g for 10 min. Supernatants and pellets were analyzed by SDS-PAGE.

Actin Filament Bundling Assay

The 6xHis tagged proteins prepared as above were mixed with actin filaments stabilized with equimolar TRITC-labeled phalloidin (Sigma Chemical Co.). Final concentrations were 3.5 μM actin and 0.2–3 μM anillin fragment. After 15 min the reactions were diluted 100-fold into PB containing 60% glycerol and 0.1% glutaraldehyde and observed immediately by fluorescence microscopy. For protein 127-371, the experiment was repeated with protein further purified by gel filtration (see below) with identical results.

Actin

The actin used for affinity chromatography, cosedimentation experiments, and bundling experiments was rabbit skeletal muscle actin prepared as in (Pardee and Spudich, 1982). Phalloidin-stabilized actin filaments were prepared by mixing G-actin with polymerization buffer (PB), 50 mM Tris, pH 7.6, 20 mM KCl, 2 mM MgCl$_2$, 0.2 mM ATP. Filaments were allowed to polymerize for 15 min at 4°C, and then stabilized with 10 μg/ml of phalloidin.

Analytical Ultracentrifugation

The 6xHis protein 127-371 was purified by Ni-NTA chromatography and then subjected to FPLC gel filtration (Superose 12; Pharmacia Fine Chemicals, Piscataway, NJ) in 50 mM Tris Cl, pH 7.7, 20 mM KCl, 2 mM MgCl$_2$, and 1 mM DTT. The protein eluted in a single, symmetrical peak. Two different fractions from this peak were subjected to equilibrium ultracentrifugation in a Beckman XL-A analytical ultra centrifuge at two different protein concentrations (20 and 30 μM). Protein molecular weight and polydispersity were determined from plots of OD$_{280}$ vs. radius using the Beckman software.

Results

Anillin Cloning and Sequencing

Mouse polyclonal antibody No. 8 (Miller et al., 1989) was used to screen *Drosophila* ovary cDNA expression library (Hay et al., 1988). Two positive clones were isolated and found to be related by Southern blot analysis. One of these was used to probe a second cDNA library (Poole et al., 1985) to obtain additional coding sequence. The 5' end of the cDNA was cloned using nested PCR as described in Materials and Methods. The products of this PCR were a ladder of four related fragments, the largest of which indicated we were missing at most 200 bp at the 5' end. The sequencing of these fragments generated an additional 165 bp of non-coding sequence.

The full-length cDNA sequence of anillin (4.029 kb) (Fig. 1) is similar in size to the transcript detected by

Figure 1. Nucleotide and deduced amino acid sequence of *Drosophila* anillin. The nucleotide and amino acid sequences are numbered above each line. The smallest his-tagged fragment that binds to actin filaments is underlined (82 amino acids). The smallest his-tagged fragment that binds and bundles actin is indicated by a dashed underline extending out from and including the 82 amino acid binding domain. Three potential nuclear localization sequences are boxed. Two SH3 binding consensus sequences are underlined with a dotted line. These sequence data are available from EMBL/GenBank/DDBJ under accession number X89858.

Northern blots (slightly less than 4.3 kb, not shown). The four nucleotides upstream of the ATG are a good match to the consensus sequence found upstream of ATG's used as initiation codons in *Drosophila*. (Cavener, 1987). There are three upstream stop codons in the frame of the predicted protein and stops in all frames at the 3' end. The remaining 0.2 kb of the message is probably accounted for by untranslated sequence at the 3' end.

In situ hybridization localizes the gene to cytological position 43DE on the polytene chromosome. The amino acid
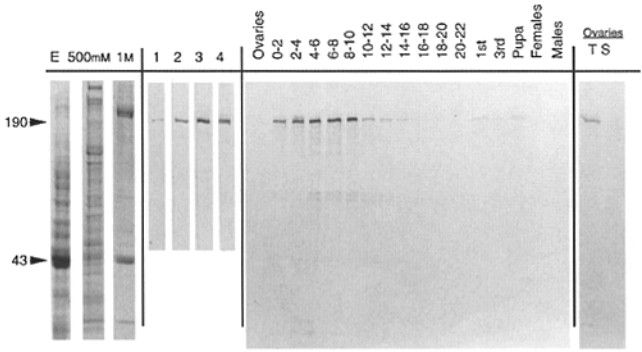
Figure 2. Immunoblot analysis of anillin. On the left are three SDS-PAGE lanes stained with Coomassie blue from an actin filament column experiment. E is embryo extract loaded on to an actin column. 500 mM and 1 M are two consecutive KCl elutions from the actin column (1 M also contains 2 mM MgCl₂ and 1 mM ATP). Anillin is a closely spaced doublet in the 500 mM elution that migrates at 190 kD. The next section (lanes 1–4) is a Western

blot characterizing the anillin antibodies used in this paper. The first three lanes are loaded with the 500 mM column elution and probed with three different anti-anillin antibodies. Lane 1 is the original mouse polyclonal serum used to screen the expression library. Lane 2 is an affinity purified rabbit sera raised against amino acids 401-828 fused to GST (GST-anillin 401-828). Lane 3 is an affinity purified rabbit sera raised against amino acids 1-371 (6xHis-anillin 1-371). Lane 4 contains Schneider cell extract probed with anti-GST-anillin 401-828. All antibodies recognize a closely spaced doublet at 190 kD. The third section is a Western blot of extracts prepared from different developmental stages as indicated above each lane. Numbers indicate embryo age in hours, 1st and 3rd indicate larval instar. Equal amounts of soluble extract protein were loaded in each lane. Note that the apparent molecular weight of the immunoreactive band is constant and that the expression levels approximately correlate with the fraction of dividing cells at each stage. The fourth section is a Western blot examining the solubility of anillin in ovaries. T is total ovary extract and S is the supernatant from a low speed spin.

| Anillin | Actin Filaments | Merged Image |
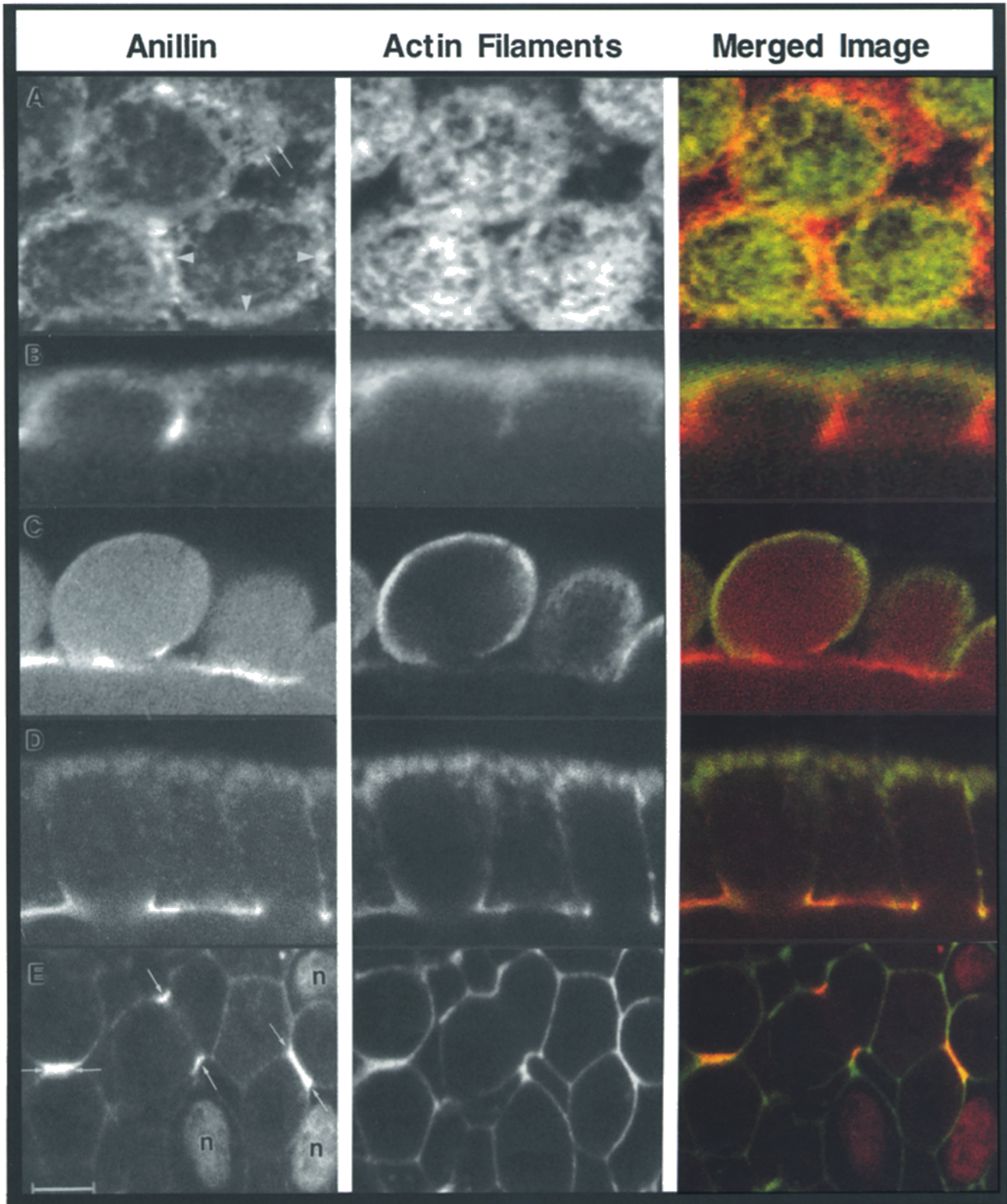
Figure 3. Confocal immunofluorescence imaging of early *Drosophila* embryos. Embryos were probed with rhodamine-anti–anillin (*anillin* column) and FITC-phalloidin (*actin* column). The column in color shows a merged image (anillin in *red*, actin filaments in *green*, colocalization in *yellow*). Row *A* shows the surface of a syncytial embryo during interphase: anillin is enriched in a ring that surrounds the actin cap (*arrowheads*) and in a meshwork between the actin caps (*arrows*). Row *B* shows a sagittal section of a syncytial embryo during prophase as the metaphase furrows begin to form: anillin is enriched in the invaginating membrane tips. Row *C* shows a sagittal section of a syncytial embryo during pole cell formation: anillin is enriched at the base of the pole cells. Row *D* shows a sagittal section of an embryo during cellularization: anillin is enriched in the invaginating membrane tips. Row *E* shows a view near the surface of a gastrulating embryo in a mitotic domain: anillin is enriched in cleavage furrows (*arrows*). Anillin is also localized in nuclei during interphase (marked *n*).

sequence predicted for anillin shows it has no significant homology to any protein in the database. Notable sequences motifs include a 300 amino acid region of relatively high proline content (amino acids 208–509, 14% proline). Contained within this region are two sequences (dotted underline) that fit the consensus for an SH3 binding site (Ren et al., 1993; Yu et al., 1994; Lim et al., 1994). There are also three sequences (boxed) that fit the consensus for a bipartite nuclear localization signal (Dingwall and Laskey, 1991).

To confirm that we had cloned the correct cDNA, rabbit polyclonal antibodies were raised against two separate portions of the protein encoded by the cDNA (for these antigen locations, see fragments with asterisks in Fig. 10 A). Affinity-purified antibodies were used for both Western blotting and immunofluorescence studies. Both the two rabbit antibodies and the original mouse antibody recognize a protein that binds to actin filament columns and runs as a closely spaced doublet of ~190 kD on SDS-PAGE (Fig. 2, lanes 1–4). All of the antibodies also recognize the same structures in Drosophila embryos and tissue culture cells, as judged by immunofluorescence.

The predicted mass of anillin is 132 kD with an isoelectric point of 5.6, though the protein migrates at 190 kD on SDS gels (Fig. 2). Mobility on SDS-PAGE slower than predicted from sequence is a common anomaly (see for example Himmler et al., 1989). Many of the proteins exhibiting this phenomenon do not fold to form typical globular proteins. At least one of our fusion proteins (fragment 354-693) also migrates larger (55 kD) than its predicted molecular weight (38 kD).

Anillin Expression

We examined anillin expression pattern by performing a developmental Western blot on low-speed supernatants of embryonic, larval and adult extracts (Fig. 2, third panel) Anillin expression was detected at all stages and its apparent molecular weight was constant. In early embryos we detected hints of an anillin species with slightly decreased gel mobility (Fig. 2, lanes 0–2 and 2–4). This might represent a phosphorylated form, but further experiments are required to address this possibility. Embryonic protein expression levels in general correlated with levels of cell divi-
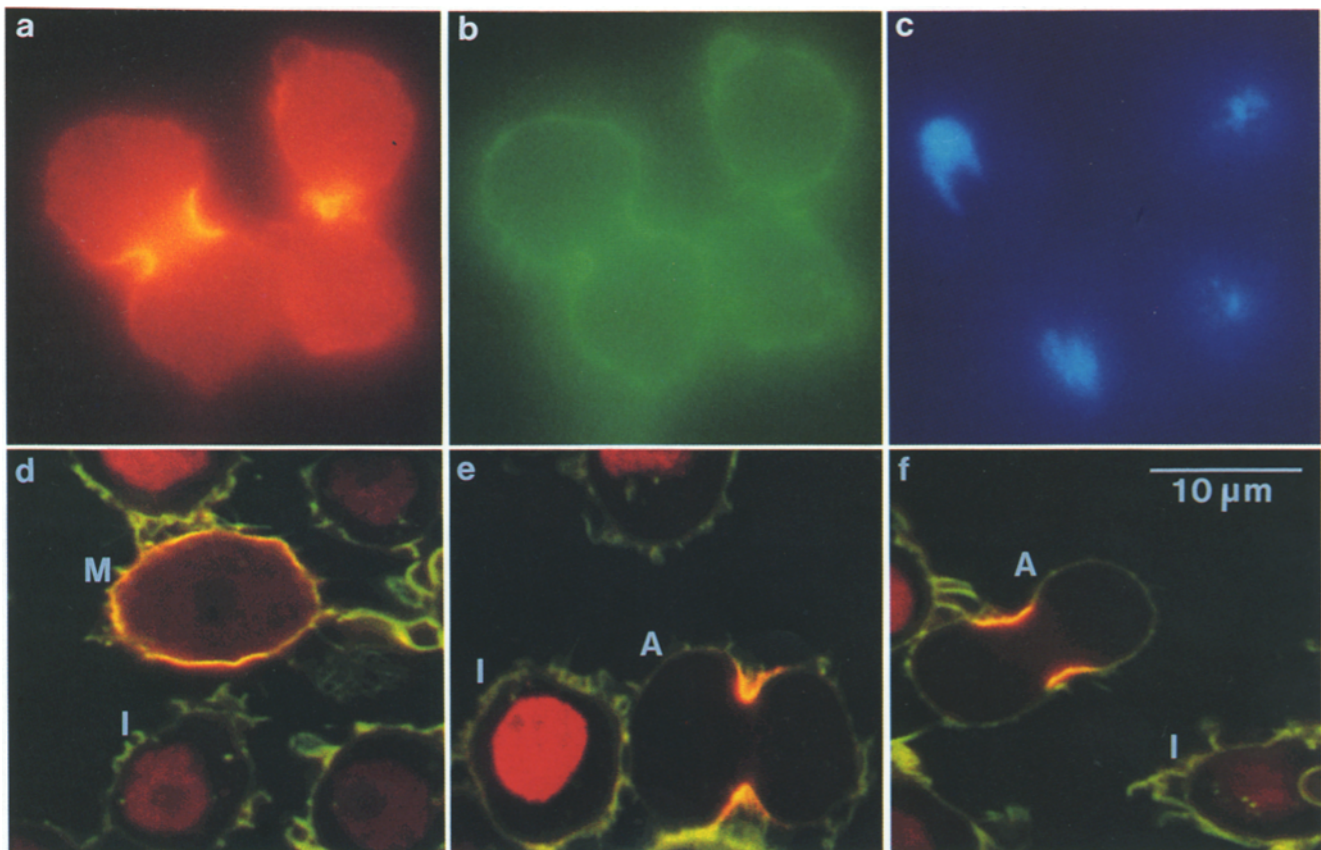
Figure 4. Anillin localization in Drosophila tissue culture cells. The top row (a–c) shows conventional immunofluorescence imaging of cells that have been probed for anillin (a, red and yellow), actin filaments (b, green), and DNA (c, blue). The cell on the left is in anaphase: anillin is enriched in the cleavage furrow. The pair of cells on the right are in late telophase: anillin is concentrated in the intercellular bridge between the two daughters. The bottom row (d–f) shows confocal immunofluorescence imaging of several fields of cells. The cells have been probed with rhodamine-anti–anillin (red) and FITC phalloidin to visualize actin (green). Areas of colocalization are shown in yellow. Individual cells have been labeled to indicate their stage in the cell cycle. Cells in interphase (I) show varying intensities of anillin staining in their nuclei. The cell in metaphase (M) in d shows anillin in the cytoplasm and colocalizing with actin filaments in the cortex. Cells in anaphase (A) show an enrichment of anillin in the cleavage furrow (e and f).

sion, being reduced later in embryogenesis. In this experiment we analyzed low-speed supernatants of embryo extracts because total embryo extract in SDS gave irreproducible gel mobility. During embryonic stages most of the anillin was soluble. However, in ovaries the low levels of anillin in the extract was in fact due to it being insoluble (Fig. 2, *last panel*). Anillin solubility in larvae, pupae, and adults was not tested.

Anillin Localization during the Syncytial Blastoderm Stages and Cellularization

Using the above antibodies, we have analysed anillin localization during the early stages of *Drosophila* embryogenesis and compared its localization to that of actin filaments. During interphase of the syncytial blastoderm stages (nuclear cycles 10 to 14), the majority of the cortical actin filaments form a cap above the nucleus. Although some anillin is found colocalizing in this cap, anillin is enriched around the cap perimeter, forming a ring near the region where the future metaphase furrow will form (Fig. 3 *A*, *arrowheads*). Some anillin is also seen in a meshwork which extends between the actin caps (Fig. 3 *A*, *arrows*). As a metaphase furrow begins to invaginate around each nucleus during prophase, anillin is highly enriched at the furrow tips (Fig. 3 *B*).

Pole cell formation, the pinching off of the progenitors of the germ cells occurs during nuclear cycle 10. This is also a specialized cleavage event (Warn et al., 1985). Actin filaments are enriched in the cortex of the nascent germ cells, while anillin is enriched in the cortex at the base of the cells. (Fig. 3 *C*). At the final stages of pinching off, a contractile-ring like staining by anillin was observed (not shown).

During cellularization, anillin is concentrated at the tips of the invaginating membranes that form the cellularization front (Fig. 3 *D*). Anillin is also enriched in the residual intercellular connections that occur at the base of each cell after the contraction that forms the individual cell is complete (not shown).

Anillin Localization in Dividing Cells

We next examined anillin localization during the cytokinesis events that occur when normal somatic cells divide during early gastrulation. In dividing cells, anillin concentrates preferentially in the cleavage furrow (Fig. 3 *E*, *arrows*). During interphase in these cells, we observed nuclear staining (Fig. 3 *E*, *n*). In all of the dividing cells we observed, during or after gastrulation, including imaginal discs and neuronal precursors, anillin was found to alternate between a nuclear localization during interphase and a cortex/cleavage furrow localization during mitosis (see also Fig. 7). This contrasts sharply with the results in earlier syncytial stage embryos, where only a cytoskeletal localization is seen.

The cell cycle dependent changes in anillin localization are particularly clear in tissue culture cells. Fig. 4 (*A–C*) shows Schneider cells triple labeled with probes for anillin (*A*), actin filaments (*B*), and DNA (*C*). Fig. 4 (*D–F*) shows several fields of cells double labeled to detect anillin (*red*) and actin filaments (*green*). Regions of colocalization ap-
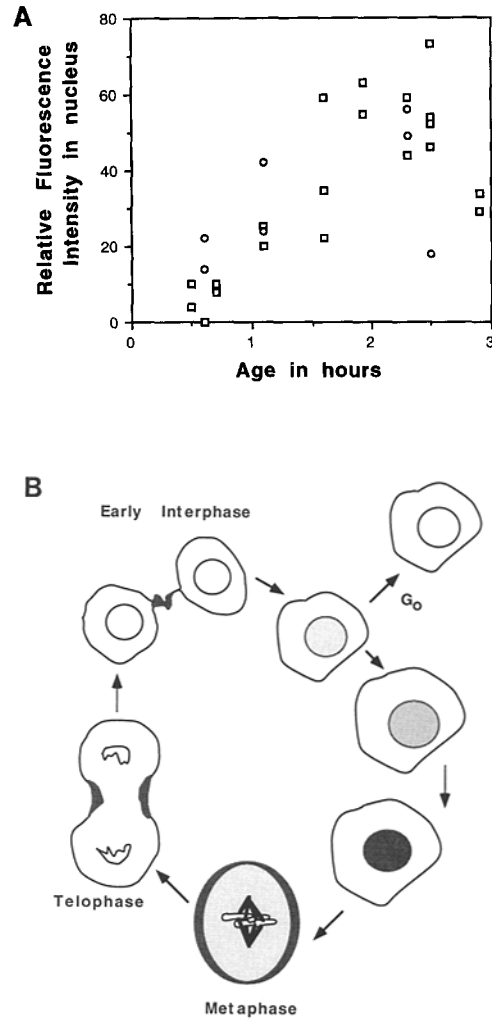
Figure 5. The cell cycle–dependent localization of anillin. (*A*) Anillin concentration in the nucleus as measured by relative fluorescence intensity is plotted with respect to the age of cell since the previous cell division. There is a direct correlation between the age of the nucleus and amount of anillin fluorescence it contains. This correlation decreases after approximately 2.5–3 h (○ Schneider cells, □ KC cells). (*B*) A model of cell cycle dependent anillin localization. Cells enter the cell cycle and begin importing anillin into their nuclei in interphase. Nuclear envelope breakdown in prophase releases anillin to the cytoplasm where it moves to the cortex. During anaphase, anillin concentrates in the area of the prospective cleavage furrow and later is enriched in the cleavage furrow. During late telophase anillin lingers in the intercellular bridge that connects the two daughter cells. Cells that pause in the cell cycle and enter G_0, degrade their anillin.

pear yellow. In interphase Schneider cells, anillin is restricted to the nucleus except for residual midbody staining in recently divided cells (Fig. 4 *A*). The intensity of the nuclear staining was strikingly variable (Fig. 4, *D–F*, *I*). Nuclear staining appeared weakest in recently divided cells (identified by their residual mid-bodies). Upon nuclear envelope breakdown at prophase, anillin becomes cytoplasmic and then moves to the actin filaments in the cortex (Fig. 4 *D*, *M*). At the onset of anaphase, anillin starts to concentrate in the area of the prospective con-
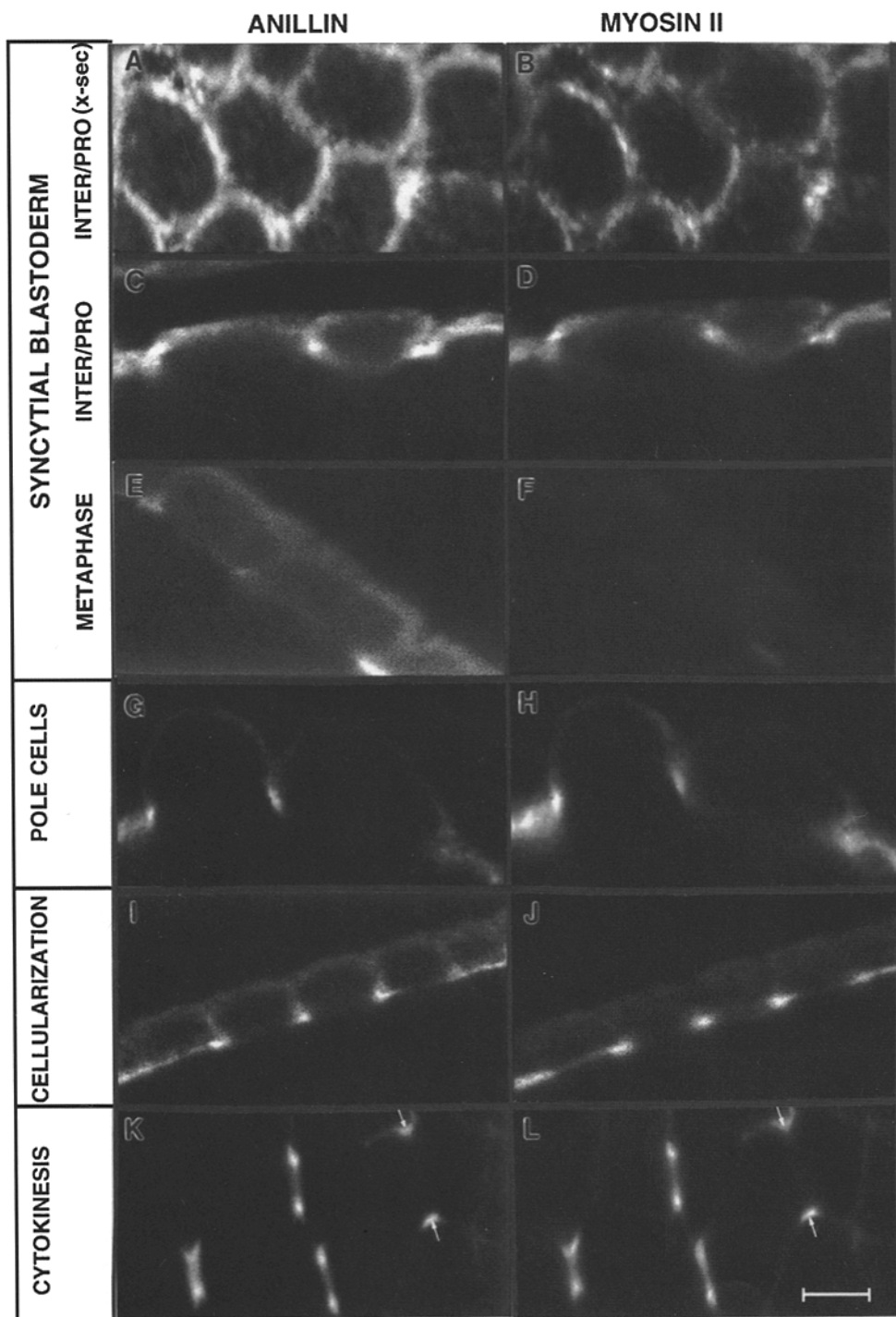
Figure 6. Confocal immunofluorescence imaging of anillin and myosin II localization in the early *Drosophila* embryo. Embryos were probed with antibodies against anillin (*left* column) and myosin II (*right* column). (Note: the cells were also probed with the DNA dye Hoechst #33258.) Panels *A–F* are from syncytial blastoderm embryos and were all taken at constant gain, black levels, and aperture settings. (*A* and *B*) Cross-section at the base of the invaginating furrow during interphase/early prophase. Anillin forms a hexagonal structure around each nucleus (nucleus is not shown in the figure) in the region where the metaphase furrow will form. Myosin II colocalizes with anillin in the hexagonal ring. (*C* and *D*) Saggital section during interphase/early prophase. Anillin and myosin II colocalize at the tips of the invaginating furrows. (*E* and *F*) Saggital section during metaphase. Anillin is concentrated at the tips of the membrane furrows. Myosin II has disppeared from the cortex. (*G* and *H*) Saggital section during pole bud formation. Anillin and myosin II colocalize at the base of the pole cells. (*I* and *J*) are a saggital section during cellularization. Anillin and myosin II colocalize at the tips of the invaginating furrows. (*K* and *L*) are a view near the surface of an embryo in a mitotic domain (cycle 14). Shown are four pairs of cells undergoing cytokinesis. Since there is no marker for actin, only the cleavage furrows can be seen. The arrow heads point to one cleavage furrow that is beginning to invaginate. Bar, 5 μm.

tractile ring, and it is restricted to the contractile ring during anaphase (Fig. 4, *E* and *F*, *A*). This pattern persists in telophase as the contractile ring pinches off, and anillin lingers in the intercellular bridge that connects the two daughter cells. In recently dividing cells, anillin begins to accumulate inside the nucleus in a diffuse staining pattern, restarting the cycle again.

To follow anillin levels more precisely during the cell cycle, we filmed *Drosophila* Schneider cells and KC cells grown on marked coverslips. We then fixed the cells and used immunofluorescence to visualize anillin. Confocal microscopy was used to quantitate the amount of fluorescence present in nuclei and to plot it with respect to the age of the cell as determined from the video record. For the first 2–3 h of interphase, there is an increase in anillin fluorescence in the nucleus (Fig. 5 *A*). After this time, the correlation between cell age and amount of anillin in the nucleus is less marked, although there is a general trend for older cells to have more anillin.

A small population of tissue culture cells has no detectable anillin in their nuclei or cytoplasm. We think that these cells are paused in G_0 phase having dropped out of

172

the cell cycle. In agreement with this idea, the percentage of these cells is higher for KC cells (grown without serum) than for Schneider cells (data not shown). In more synchronously dividing population of cells, such as the follicle cells surrounding early stage egg chambers or the mitotic domains during gastrulation, neighboring nuclei exhibit very similar levels of anillin staining. A schematic summary of the cell cycle dependent localization of anillin is presented in Fig. 5 B.

Anillin Colocalizes with Myosin II in the Contractile Rings Responsible for Cell Division

We have compared anillin localization with the localization of cytoplasmic myosin II (using an antibody kindly donated by D. Kiehart (Duke University Medical Center, Durham, NC); Kiehart and Feghali, 1986). During interphase of the syncytial blastoderm stages, anillin and myosin II colocalize on either side of the nucleus at the base of the somatic bud (this stage corresponds to Fig. 3 A). During prophase, when metaphase furrows begin to form, anillin and myosin II colocalize at the invaginating membrane tip shown in cross-section (Fig. 6, A and B) and in sagittal section (Fig. 6, C and D). Later at metaphase, anillin is still localized to the membrane tips, while myosin II staining has largely disappeared from the cortex (Fig. 6, E and F). As mitosis proceeds, the metaphase furrows retract, anillin remains at the tips although it is more diffuse (not shown).

During pole cell formation (Fig. 6, G and H), cellularization (Fig. 6, I and J), and cytokinesis (Fig. 6, K and L), anillin and myosin II colocalize. Unlike anillin, myosin II does not enter the nucleus of dividing cells in the embryo.

Anillin does not colocalize with myosin II in the apically constricting tips of cells at the leading edge during dorsal closure (Fig. 7). This cell shape change is thought to be caused by an actin/myosin II contraction (Young et al.,
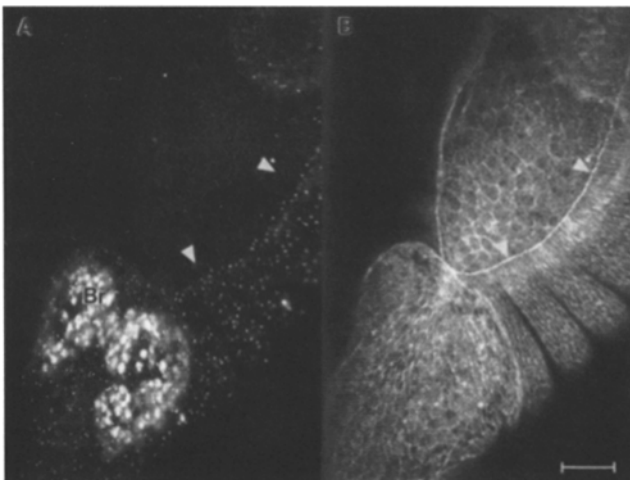

Figure 7. Confocal immunofluorescence imaging of anillin (*A*) and myosin II (*B*) localization during dorsal closure. Anillin does not colocalize with myosin II in the apically contricting cells at the leading edge during dorsal closure (see *arrowheads*). Anillin is expressed and cycling from the nuclei to the cortex in the cells dividing to form the brain (*Br*). Note that anillin is also present in small spots that we postulate are residues of completed contractile rings. Bar, 30 μM.

1993). No anillin protein can be seen in these cells by immunofluorescence. Anillin is seen in small spots scattered through out the late embryo. Myosin II does not colocalize with the majority of these spots.

Anillin Localization in Ovarioles

The location of anillin during oogenesis is compared to that of actin filaments and DNA in Fig. 8. In early egg chambers, anillin is concentrated in the arrested cleavage furrows that link the oocyte to its 15 nurse cells (Fig. 8 *e*). These intercellular connections later differentiate into the ring canals that allow bulk transport of materials from the nurse cells to the oocyte. As the arrested furrows transform into ring canals, they gradually lose their anillin. The disappearance of anillin, which is almost complete at egg chamber stage 2 (Fig. 8 *e*), coincides with the time that the ring canals acquire both their mature ultrastructure (King et al., 1982) and specialized actin binding proteins (Robinson et al., 1994).

The follicle cells that surround the egg chambers in the ovarioles initially divide rapidly to maintain a continuous monolayer around an egg chamber of increasing size. In stage 6 egg chambers, this cell division ceases. The follicle cells become polyploid and continue to increase in size (Spradling, 1993). Anillin cycles from the nucleus to the cleavage furrow in the follicle cells surrounding egg chambers through stage 5. However, the cessation of cell division (in stage 6 and older egg chambers) is accompanied by a dramatic loss of anillin staining in follicle cell nuclei (Fig. 8 *b*). The polyploid nurse cell nuclei never accumulate anillin in their nuclei, even though anillin protein is present in the nurse cell cytoplasm (Fig. 8 *b*). Comparing data from ovarioles and late stage embryos we conclude that anillin localizes to nuclei only in dividing cells, and the presence of anillin in the nucleus appears to be a good marker for a cell's potential to divide.

Anillin Binds to and Bundles Actin Filaments

To determine whether anillin binds directly to actin filaments, we used protein A beads coated with anillin antibody to immunoprecipitate the endogenous protein. Phalloidin-stabilized actin filaments were added to these beads and then sedimented at low speed through a sucrose gradient. Proteins sedimenting with the beads were analyzed by SDS-PAGE. Fig. 9 shows the results of such an experiment. Anillin sediments from embryo extract with both anti-anillin antibodies (Fig. 9, lanes *1* and *2*). Anillin does not sediment with random rabbit IgG (lane *3*). Actin filaments added to the antibody loaded beads cosediment with the anillin bound beads (lanes *4* and *5*) but not with control beads bound with random rabbit IgG (lane *6*).

We used fragments of bacterially expressed anillin to map the actin binding domain of anillin. Initially, the entire predicted protein sequence was divided into five segments by PCR methods and expressed as fusion proteins with a fourteen amino acid tag at their NH₂ terminus. This tag includes six histidines that permit each fusion protein to be purified on immobilized nickel columns. Fig. 10 A shows the five 6xHis tagged fragments (plus one GST fusion protein) that were initially tested for actin binding.

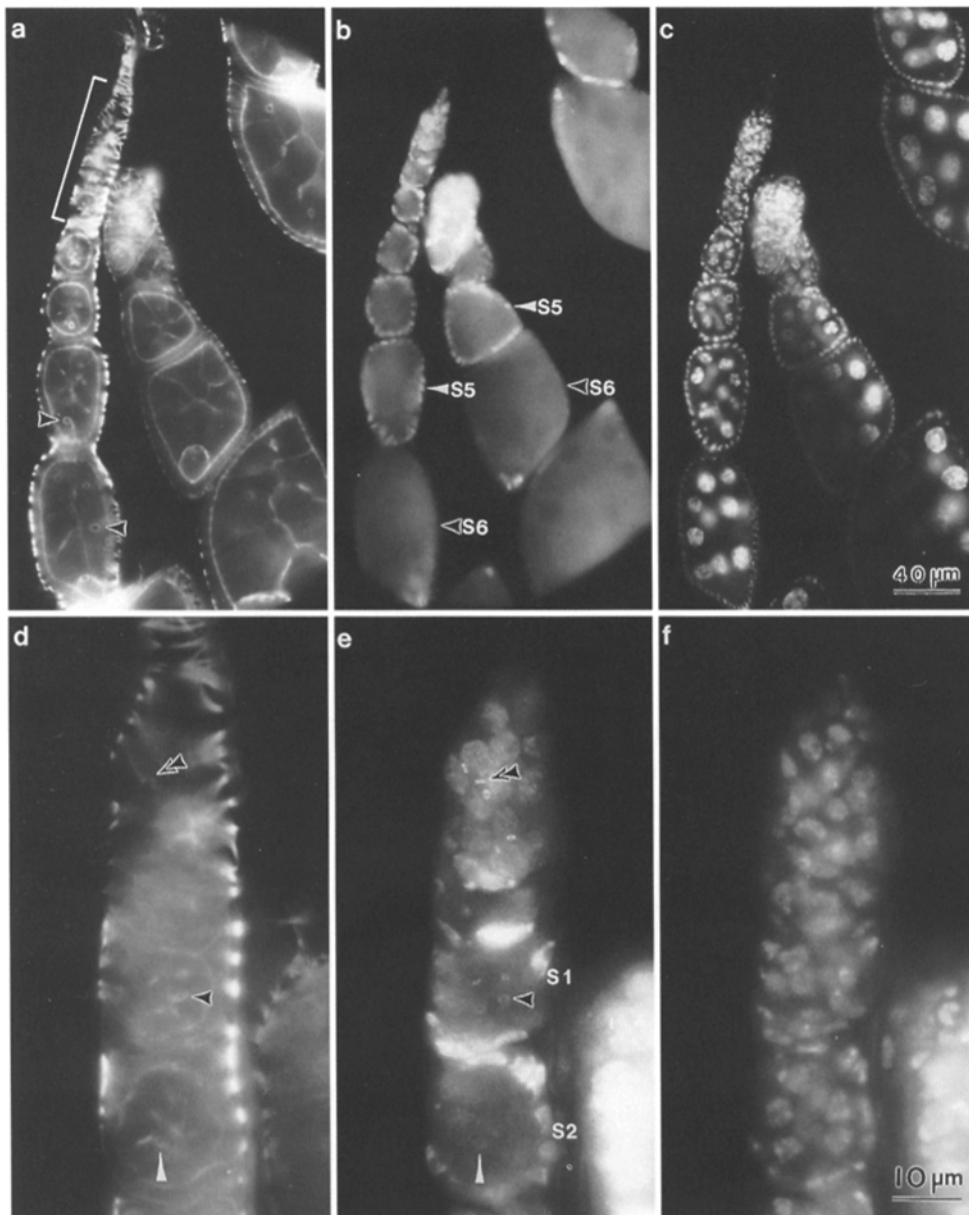Purified fusion proteins were passed over both actin fila-

Figure 8. Conventional immunofluorescence analysis of anillin localization in ovarioles. The *Drosophila* ovary is divided into discrete units called ovarioles (*a–c*). At the anterior end of the ovariole is the germarium. (Shown in brackets in *a* and enlarged in *d–f*). The germarium is connected to a series of egg chambers that mature as they move posteriorly. The youngest egg chamber is termed stage 1 (*S1*). An egg chamber consists of three cell types; an oocyte, nurse cells, and follicle cells. Each oocyte is interconnected to 15 nurse cells by structures called ring canals. The follicle cells surround the oocyte/nurse cell complex and divide as the egg chamber matures and increases in size. They continue to divide through egg chamber stage 5 (*S5*). During stage 6 (*S6*), the follicle cell nuclei stop dividing and become polyploid. Panels *a* and *d* are probed with FITC-phalloidin to visualize actin filaments. Panels *b* and *e* are probed with rhodamine-anti–anillin. Panels *c* and *f* are probed with the DNA dye, Hoechst #33258. Anillin enters the nuclei of follicle cells which are dividing (through stage 5), however in stage 6 when the cells stop dividing, anillin no longer enters the nucleus. (See panel *b*, compare *white arrowheads* [*S5*] with *black arrowheads* [*S6*]). The images in panels *d* and *e* show that anillin is present in the immature ring canals (*double black arrowheads* in *d*). Anillin gradually disappears as actin intensity increases (*long white arrowheads*). Note that anillin does not colocalize with the majority of filamentous actin structures.

ment columns and control albumin columns. The columns were then washed extensively and eluted with 0.5 M KCl. The fragment that contained the amino terminal 371 amino acids of anillin bound quantitatively to actin filament columns, while passing through the control column. None of the other fragments bound to either column (not shown).

The actin binding portion of anillin was further defined by preparing shorter fusion proteins shown in Fig. 10 *B*. To test for actin binding, the fusion proteins in Fig. 10 *B* were incubated with phalloidin-stabilized actin filaments and sedimented through a 40% glycerol cushion. The su-

pernatants and pellets were analyzed by SDS-PAGE. Fig. 11 displays the results of such a sedimentation experiment. The first two panels show the data for anillin fragments that cosediment with actin filaments and the third and fourth panels for anillin fragments that do not co-sediment. The chart in Fig. 10 *B* summarizes the results of these binding studies. All fragments that bind have an 82-amino acid fragment in common. This fragment on its own is also capable of binding actin filaments.

We have tested the salt sensitivity of the actin-binding for several of the protein fragments in Fig. 10 *B*. Sedimentation experiments show that the binding is decreased in
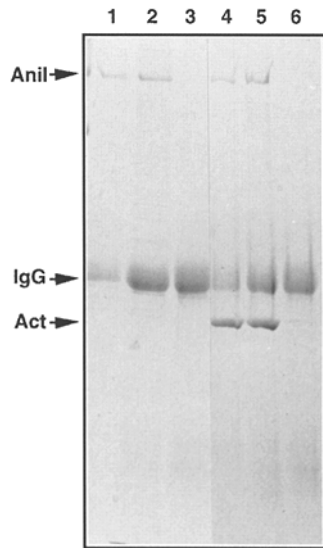
Figure 9. Coomassie stained gel analysis of endogenous anillin binding directly to actin filaments. Lanes *1* and *2* show that anillin labeled (*Anil*) from embryo extracts binds to protein A beads coated with two different anti–anillin antibodies (anti-6xHis-anillin 1-371 (lane *1*) and anti-GST-anillin 401-828 (lane *2*). Beads coated with random rabbit IgG do not bind anillin (lane *3*). Lanes *4–6* show the result of adding phalloidin-stabilized actin filaments to the antibody coated beads and then sedimenting these beads through a sucrose cushion. Actin filaments (*Act*) cosediment with beads that have bound anillin (lanes *4* and *5*) and not with control coated beads (lane *6*). Note the antibodies are in the same order as in lanes *1–3*.

Figure 11. An analysis of actin filament cosedimentation experiments by SDS-PAGE. Each of the four fusion proteins was tested for cosedimentation with actin filaments (*F-actin*) (left pair of lanes in each panel) or alone (right pair of lanes). The arrowhead marked A indicates actin. The arrowhead without an A marks the position of the fusion protein. *S*, supernatant. *P*, pellet. Fragments 127-371 and 204-371 bind to actin filaments. Fragments 1-209 and 1-126 do not. The chart in Fig. 10 *B* summarizes the results of these experiments.

the presence of 200 mM but not 150 mM KCl (200 mM is the salt concentration that starts to elute anillin from the actin filament columns). However, even at 400 mM KCl, some of the protein still sediments with the actin filaments (not shown).

To test the actin-binding fragments for their effect on actin filaments, purified fusion proteins were mixed with
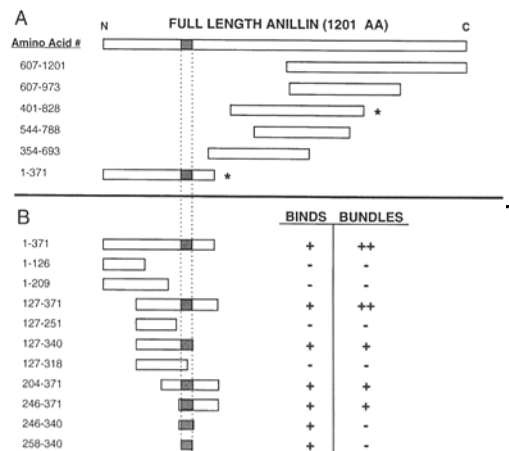

Figure 10. Schematic of the full length protein sequence of anillin and the fragments generated using PCR to test for actin filament binding. (*A*) The fragments tested for actin binding in column experiments. Fragment 1-371 bound quantitatively to actin filament columns and not to albumin control columns. The * indicates fragments that were used as antigens. (*B*) The fragments tested for actin binding by cosedimentation experiments. On the right, the results of the binding and bundling studies have been summarized in chart form. The ++ under bundling indicates that the fragment bundles stably in the presence of 100 mM KCl. The stippled box indicates 82 amino acids that are in common in all proteins that cosedimented with actin filaments. All fragments have 6xHis tags except 401-828, which is a GST fusion protein.
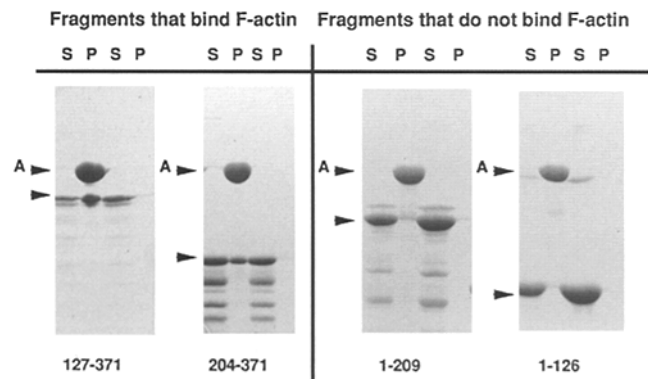
actin filaments stabilized with rhodamine-labeled phalloidin and visualized by fluorescence microscopy. A pronounced bundling of the actin filaments was observed with several of the protein fragments in the presence of 50 mM KCl as shown in Fig. 12. When the KCl concentration was raised to 100 mM, bundling disappeared for some fragments, and only the bundling by fragments 1-371 and 127-371 was unaffected. The actin filament bundling activities observed are summarized in the chart in Fig. 10 *B*.

This bundling of actin filaments requires that an anillin fragment contain two or more actin binding sites. Alternatively, the protein could act as a dimer or multimer with a single site per monomer (Matudaira, 1991). To distinguish between these two possibilities, fusion protein 127-371, the smallest of the fragments that binds and bundles stably in the presence of 100 mM KCl was analyzed by sedimentation equilibrium in an analytical ultracentrifuge. The molecular weight of the native anillin fragment was estimated at 30.5, 29.5, and 31 kD in three different runs at two different protein concentrations. These values are similar to the predicted monomer size of 28.1 kD. The centrifugation was performed at higher protein concentrations (20–30 μm) than the bundling assay (3 μm), so it is unlikely that the protein was dimerized under the conditions of the assay. We conclude that this protein fragment bundles as a monomer, consistent with the idea that the 127-371 fragment contains two separate actin binding sites. However, we cannot exclude the possibility that anillin may dimerize only after binding to actin filaments.

Discussion

One approach to understanding the mechanism and regulation of cytokinesis is to identify proteins that comprise the cleavage furrow, and to study their functions and interactions individually. Actin-filament affinity chromatography combined with immunocytochemistry has proven successful in identifying novel actin binding proteins. By
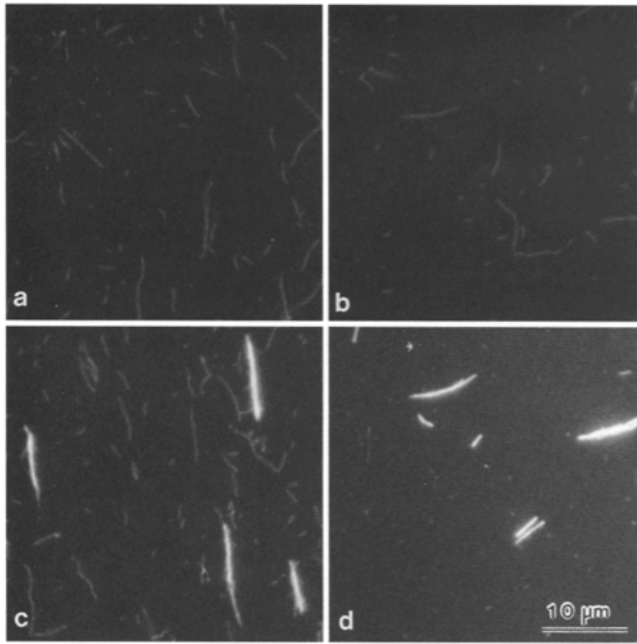
Figure 12. Immunofluorescence analysis of actin filament bundling experiments. (*a*) Fluorescent actin alone. (*b*) Fluorescent actin with non binder 1-209. (*c*) Fluorescent actin with fragment 127-371. (*d*) Fluorescent actin with fragment 246-371. For details see Materials and Methods. Bundling is seen in only *c* and *d*. The chart in Fig. 10 *B* summarizes the results of these experiments.

focusing on proteins enriched in the invaginating furrow tips during early embryonic contractile events, we have identified a novel protein, anillin, that is also enriched in the cleavage furrows of all dividing *Drosophila* cells. We have identified three other furrow enriched actin binding proteins using this strategy (Field, C., unpublished results). Two of them are previously identified actin binding proteins, myosin II, which is known to be central to the cleavage mechanism (Satterwhite and Pollard, 1992), and the *Drosophila* homologue of ABP 280 which has been implicated in the maintenance of cortical integrity (Cunningham et al., 1992; Gorlin et al., 1990). The third protein appears to be novel.

Anillin Sequence

The predicted amino acid sequence of anillin provides little information regarding the function of the protein. It contains a proline-rich region, as do several other actin binding and cytoskeletal proteins: c-abl (Van Etten et al., 1994), radixin (Funayama et al., 1991), ABP 1 (Drubin et al., 1990), and Z-01 (Bement et al., 1993). Included within the proline rich region of anillin are two consensus sequences for an SH3 binding domain (Fig. 1, *dotted underline*) (Yu et al., 1994; Lim, et al., 1994). SH3 domains are contained in other cytoskeletal and membrane-associated proteins, including myosin I (Drubin et al., 1990) and are thought to mediate protein–protein interactions (Ren et al., 1993). Anillin also contains at least three possible nuclear localization sequences (Fig. 1, *boxed*). We have not yet tested whether these sequences are responsible for the nuclear localization of anillin. The region of anillin that binds and bundles actin filaments in our in vitro studies

(amino acids 127-371) has no obvious homology with other known actin binding domains.

Anillin Localization in Contractile Domains

It may be useful to think of the actin cytoskeleton in the early *Drosophila* embryo as organized into two types of domains, contractile domains that are rich in myosin II, and noncontractile domains that consist of the majority of the cortical actin filaments in the cell. Anillin is associated preferentially with actin filaments in contractile domains such as the contractile ring formed during cellularization or cytokinesis.

While it has been generally accepted that cellularization is a specialized form of cytokinesis, the mechanism responsible for the contractile events occuring in the syncytial embryo have been less clear. Our anillin/myosin II colocalization data is consistent with a common mechanism for all the contractile events associated with the isolation of two parts of the cytoplasm from one another. We term such events "cell division associated contractivity." In *Drosophila*, these events include; pole bud formation, somatic budding, metaphase furrow formation, cellularization, and cytokinesis. Interestingly, anillin is absent from the apically contracting tips of cells at the leading edge during dorsal closure, though myosin II is highly enriched in these contractile structures. This implies mechanistic differences in the regulation of cell division associated contractile events and contractile events associated with cell shape changes in interphase.

Implicit in our observations in the syncytial embryo is a revised view of when the contraction occurs during metaphase furrow formation. We propose that the active contractile event during nuclear cycles 10–13 occurs during interphase and prophase, when anillin and myosin II are both greatly enriched on either side of the nucleus. We postulate that an actin/myosin based contraction creates the somatic buds seen during interphase and later the metaphase furrows, which are actually formed during prophase. The absence of myosin II from the tips of the furrows during metaphase suggests that once the contraction is complete, myosin is no longer required and disappears from the cortex. Anillin persists in the metaphase furrow through mitosis, and remains associated as the cortex relaxes during telophase.

The strong enrichment of anillin in cell division associated contractile domains of the actin cytoskeleton suggests that it plays a role in their organization or function. Our in vitro data indicates that anillin can bundle actin filaments. Thus one potential role for anillin is to mechanically stabilize actin filaments during contraction. Another bundling protein, α-actinin, localizes to contractile rings, but its enrichment in these structures is variable (Satterwhite and Pollard, 1992).

In all the cell division associated contractile events we have studied (nascent ring canals, metaphase furrows, and cytokinesis) anillin persists at the region of membrane furrowing after contraction has finished and myosin II has released from the cortex. Thus anillin may play a role in stabilizing the membrane invagination after myosin II–mediated force production ceases by bundling cortical actin. In situations where cyokinesis occurs to completion (i.e., the in-

vaginating membranes fuse) anillin may play a role in the completion step. Little is known about the mechanisms of this step, in which the septin proteins have also been suggested to play a role (Sanders and Field, 1994). In situations where cytokinesis is incomplete, such as ring canals, anillin may serve to cross-link the actin filaments supporting the invaginated cortex until more permanent cross-linking proteins such as kelch (Robinson et al., 1994) are recruited.

Anillin Localization in the Nucleus

In later embryonic and tissue culture cells, anillin resides in the nucleus during the majority of the cell cycle, separated from the actin cytoskeleton (see Fig. 3 *E* and Fig. 4, *D-F*). The mechanism of nuclear enrichment of anillin is unknown, although its sequence contains three potential nuclear localization sequences (NLSs). A NLS that is active during interphase and dominant over other localization signals, combined with one or more actin binding sites that are active during mitosis, could account for the cycling of anillin between nucleus and cortex.

We speculate that the nuclear localization of anillin serves to prevent the protein's interaction with cortical actin. Release of anillin from the nucleus during mitosis could play a role in organizing the cortex for its specialized function in cleavage. Anillin could thus play a role in coordinating the cytoskeletal changes that occur during cell division with respect to the cell cycle. Consistent with this idea, anillin is only expressed in cells with the potential to divide with the exception of nurse cells, where is is presumably stock-piled for later use in embryogenesis. An alternative view would be that anillin plays an active role in the nucleus, a possibility that might be most readily tested by genetic analysis.

In the precellularization embryo, anillin never enters nuclei although other nuclear proteins such as histones (Minden et al., 1989) and topoisomerase II (Swedlow et al., 1993) are efficiently imported during this stage. The timing of cell division associated contractivity is different in syncytial blastoderm embryos compared to somatic cells, where cytokinesis occurs in anaphase. Cytoplasmic buds protrude in interphase and metaphase furrows begin to form in prophase. The membrane invaginations that occur during cellularization also form during interphase (Foe and Alberts, 1983; Karr and Alberts, 1986). Nuclear uptake of anillin may be inactivated in precellularization embryos to allow anillin to interact with the interphase cortex, or cortical binding may be dominant over nuclear uptake. The change to the more typical regulation with nuclear uptake in interphase may require zygotic transcription.

How anillin becomes localized to a subset of the cell's actin filaments in contractile domains is not known. The same question can be asked for myosin, peanut, radixin, and other actin binding proteins that localize to contractile rings. Binding specificity of anillin could be conferred by local regulation of actin-binding activity, for example by phosphorylation. Alternatively, selective localization may arise from direct interaction between anillin and other furrow proteins, such as myosin II or peanut. The actin binding domain of anillin accounts for only a small part of the protein (~20%). Other domains of the molecule are likely

to be important for both its function and its localization. Preliminary biochemical experiments have not detected high affinity interactions between anillin and myosin or other proteins. However affinity chromatography on immobilized anillin has identified several interacting proteins (unpublished results of Field, C.). Their identification and characterization may help us to better understand how furrows function and are formed.

References

Bement, W. M., P. Forscher, and M. S. Mooseker. 1993. A novel cytoskeletal structure involved in purse string wound closure and cell polarity maintenance. *J. Cell Biol.* 121:565–578.

Brown, N. H., and F. C. Kafatos. 1988. Functional cDNA libraries from *Drosophila* embryos. *J. Mol. Biol.* 116:1431–1442.

Cavener, D. R. 1987. Comparison of the consensus sequence flanking translated start sites in *Drosophila* and vertebrates. *Nucleic Acids Res.* 15:1353–1361.

Cunningham, C. C., J. B. Gorlin, D. J. Kwiatkowski, J. H. Hartwig, P. A. Janmey, H. R. Byers, and T. P. Stossel. 1992. Actin-binding protein requirement for cortical stability and efficient locomotion. *Science (Wash. DC).* 255:325–327.

Dingwall, C., and R. A. Laskey. 1991. Nuclear targeting sequences—a consensus? *Trends Biochem. Sci.* 16:478–481.

Drubin, D. G., J. Mulholland, Z. M. Zhu, and D. Botstein. 1990. Homology of a yeast actin-binding protein to signal transduction proteins and myosin-I. *Nature (Lond.).* 343:288–290.

Foe, V. E. 1989. Mitotic domains reveal early commitment of cells in *Drosophila* embryos. *Development.* 107:1–22.

Foe, V. E., and B. M. Alberts. 1983. Studies of nuclear and cytoplasmic behavior during the five mitotic cycles that precede gastrulation in *Drosophila* embryogenesis. *J. Cell Sci.* 61:31–70.

Foe, V. E., G. M. Odell, and B. A. Edgar. 1993. Mitosis and morphogenesis in the *Drosophila* embryo: point and counterpoint. *In* The Development of *Drosophila* melanogaster. Vol. 1. M. Bate, and A. F. Arias, editors. Cold Spring Harbor Press, Plainview, NY. 149–300.

Funayama, N., A. Nagafuchi, N. Sato, S. Tsukita, and S. Tsukita. 1991. Radixin is a novel member of the band 4.1 family. *J. Cell Biol.* 115:1039–1048.

Gibbons, I. R., D. J. Asai, N. S. Chung, G. J. Doleki, G. Mocz, C. A. Phillipson, H. Ren, W. J. Tang, and B. H. Gibbons. 1991. A PCR approach to determine the sequence of large polypeptides by rapid walking through a cDNA library. *Proc. Natl. Acad. Sci. USA.* 88 (19):8563–8567.

Gorlin, J. B., R. Yamin, S. Egan, M. Stewart, T. P. Stossel, D. J. Kwiatkowski, and J. H. Hartwig. 1990. Human endothelial actin-binding protein (ABP-280, nonmuscle filamin): a molecular leaf spring. *J. Cell Biol.* 111:1089–1105.

Hay, B., L. Y. Jan, and Y. N. Jan. 1988. A protein component of *Drosophila* polar granules is encoded by vasa and has extensive sequence similarity to ATP-dependent helicases. *Cell.* 55:577–587.

Hime, G., and R. Saint. 1992. Zygotic expression of the pebble locus is required for cytokinesis during the postblastoderm mitoses of *Drosophila. Development.* 114:165–171.

Himmler, A., D. N. Drechsel, M. W. Kirschner, and D. W. Martin. 1989. Tau consists of a set of proteins with repeated C-terminal microtubule-binding domains and variable N-terminal domains. *Mol. Cell. Biol.* 9:1381–1388.

Huynh, T. V., R. A. Young, and R. W. Davis. 1985. Constructing and screening cDNA libraries in lambda gt10 and lambda gt11. *In* DNA Cloning: A Practical Approach. Vol. 1. D. Glover, editor. IRL Press, Oxford, UK. 49–78.

Janknecht, R., G. de Maartynoff, J. Lou, R. A. Hipskind, A. Nordheim, and H. G. Stunnenberg. 1991. Rapid and efficient purification of native histidine-tagged portion expressed by recombinant vaccinia virus. *Proc. Natl. Acad. Sci. USA.* 88:8972–8976.

Karr, T. L., and B. M. Alberts. 1986. Organization of the cytoskeleton in early *Drosophila* embryos. *J. Cell Biol.* 102:1494–1509.

Kellerman, K. A., and K. G. Miller. 1992. An unconventional myosin heavy chain gene from *Drosophila melanogaster. J. Cell Biol.* 119:823–834.

Kellogg, D. R., C. M. Field, and B. M. Alberts. 1989. Identification of microtubule-associated proteins in the centrosome, spindle, and kinetochore of the early *Drosophila* embryo. *J. Cell Biol.* 109:2977–2991.

Kiehart, D. P., and R. Feghali. Cytoplasmic myosin from *Drosophila melanogaster. J. Cell. Biol.* 103:1517–1525.

King, R. C., J. D. Cassidy, and A. Roussett. The formation of clones of interconnected cells during oogenesis in insects. *In* Insect Ultrastructure. Vol. 1. R. C. King and H. Akai, editors. Plenum Press, NY. 3–31.

Lehner, C. F. 1992. The pebble gene is required for cytokinesis in *Drosophila. J. Cell Sci.* 103:1021–1030.

Lim, W. A., F. M. Richards, and R. O. Fox,. 1994. Structural determinants of peptide-binding orientation and of sequence specificity in SH3 domains. *Nature (Lond.).* 372:375–379.

Matudaira, P. 1991. Modular organization of actin crosslinking proteins. *Trends Biochem. Soc.* 16:87–92.

Miller, K. G., C. M. Field, and B. M. Alberts. 1989. Actin-binding proteins from *Drosophila* embryos: a complex network of interacting proteins detected by F-actin chromatography. *J. Cell Biol.* 109:2963–2975.

Miller, K. G., C. M. Field, D. R. Kellogg, and B. M. Alberts. 1991. Use of actin filament and microtubule affinity chromatography to identify proteins that bind to the cytoskeleton. *Methods Enzymol.* 196:303–319.

Minden, J. S., D. A. Agard, J. W. Sedat, and B. M. Alberts. 1989. Direct cell lineage analysis in *Drosophila melanogaster* by time-lapse, three-dimensional optical microscopy of living embryos. *J. Cell Biol.* 109:505–516.

Neufeld, T. P., and G. M. Rubin. 1994. The *Drosophila* peanut gene is required for cytokinesis and encodes a protein similar to yeast putative bud neck filament proteins. *Cell.* 77:371–379.

Pardee, J. D., and J. A. Spudich. 1982. Purification of muscle actin. *Methods Enzymol.* 85:164–181.

Poole, S. J., L. M. Kauvar, B. Drees, and T. Kornberg. 1985. The engrailed locus of *Drosophila*: structural analysis of an embryonic transcript. *Cell.* 40:37–43.

Postner, M. A., K. G. Miller, and E. F. Wieschaus. 1992. Maternal effect mutations of the sponge locus affect actin cytoskeletal rearrangements in *Drosophila melanogaster* embryos. *J. Cell Biol.* 119:1205–1218.

Rappaport, R., and B. N. Rappaport. 1974. Establishment of cleavage furrows by the mitotic spindle. *J. Exp. Zool.* 183:115–119.

Ren, R., B. J. Mayer, P. Cicchetti, and D. Baltimore. 1993. Identification of a ten-amino acid proline-rich SH3 binding site. *Science (Wash. DC).* 259:1157–1161.

Robinson, D. R., K. Cant, and L. Cooley. 1994. Morphogenesis of *Drosophila* ovarian ring canals. *Development.* 120:2015–2025.

Rose, L. S., and E. Wieschaus. 1992. The *Drosophila* cellularization gene nullo produces a blastoderm-specific transcript whose levels respond to the nucleocytoplasmic ratio. *Genes & Dev.* 6:1255–1268.

Salmon, E. D. 1989. Cytokinesis in animal cells. *Curr. Opin. Cell Biol.* 1:541–547.

Sambrook, J., E. F. Fritsch, and T. Maniatis. 1989. Molecular Cloning: A Laboratory Manual. Second edition. Cold Spring Harbor Laboratory, Cold Spring Harbor, NY.

Sanders, S. L., and C. M. Field. 1994. Septins in common? *Curr. Biol.* 4:907–910.

Satterwhite, L. L., and T. D. Pollard. 1992. Cytokinesis. *Curr. Opin. Cell Biol.* 4:43–52.

Schejter, E. D., and E. Wieschaus. 1993*a*. Bottleneck acts as a regulator of the microfilament network governing cellularization of the *Drosophila* embryo. *Cell.* 75:373–385.

Schejter, E. D., and E. Wieschaus. 1993*b*. Functional elements of the cytoskeleton in the early *Drosophila* embryo. *Annu. Rev. Cell Biol.* 9:67–99.

Schweisguth, F., J. A. Lepesant, and A. Vincent. 1990. The serendipity alpha gene encodes a membrane-associated protein required for the cellularization of the *Drosophila* embryo. *Genes & Dev.* 4:922–931.

Smith, D. B. 1988. Single-step purification of polypeptides expressed in *Escherichia coli* as fusions with glutathione S-transferase. *Gene.* 67:31–40.

Spradling, A. C. 1993. Developmental genetics of oogenesis. *In* The Development of *Drosophila melanogaster.* Vol. 1. M. Bate, and A. M. Arias, editors. Cold Spring Harbor Laboratory Press, Plainview, NY. 1–70.

Sullivan, W., P. Fogarty, and W. Theurkauf. 1993. Mutations affecting the cytoskeletal organization of syncytial *Drosophila* embryos. *Development.* 118:1245–1254.

Sullivan, W., J. S. Minden, and B. M. Alberts. 1990. daughterless-abo-like, a *Drosophila* maternal-effect mutation that exhibits abnormal centrosome separation during the late blastoderm divisions. *Development.* 110:311–323.

Swedlow, J. R., J. W. Sedat, and D. A. Agard. 1993. Multiple chromosomal populations of topoisomerase II detected *in vivo* by time-lapse, three-dimensional wide-field microscopy. *Cell.* 73:97–108.

Theurkauf, W. E. 1992. Behavior of structurally divergent alpha-tubulin isotypes during *Drosophila* embryogenesis: evidence for post-translational regulation of isotype abundance. *Dev. Biol.* 154:205–217.

Theurkauf, W. E., S. Smiley, M. L. Wong, and B. M. Alberts. 1992. Reorganization of the cytoskeleton during *Drosophila* oogenesis: implications for axis specification and intercellular transport. *Development.* 115:923–936.

Thomas, G., and D. P. Kiehart. 1994. Beta Heavy-spectrin has a restricted tissue and subcellular distribution during *Drosophila* embryogenesis. *Development.* 120:2039–2050.

Van Etten, R. A., P. K. Jackson, D. Baltimore, M. C. Sanders, P. T. Matsudaira, and P. A. Janmey. 1994. The COOH terminal terminus of the c-Abl tyrosine kinase contains distinct F- and G-actin binding domains with bundling activity. *J. Cell Biol.* 124:325–340.

Warn, R. M., and M. Robert-Nicoud. 1990. F-actin organization during the cellularization of the *Drosophila* embryo as revealed with a confocal laser scanning microscope. *J. Cell Sci.* 96:35–42.

Warn, R. M., L. Smith, and A. Warn. 1985. Three distinct distributions of F-actin occur during the divisions of polar surface caps to produce pole cells in *Drosophila* embryos. *J. Cell Biol.* 100:1010–1015.

Young, E. E., A. M. Richman, A. S. Ketchum, D. P. Kiehart. 1993. Morphogenesis in Drosophila requires nonmuscle myosin heavy chain function. *Genes & Dev.* (1):29–41.

Young, P. E., T. C. Pesacreta, and D. P. Kiehart. 1991. Dynamic changes in the distribution of cytoplasmic myosin during *Drosophila* embryogenesis. *Development.* 111:1–14.

Yu, H., J. K. Chen, S. Feng, D. C. Dalgarno, A. W. Brauer, and S. L. Schreiber. 1994. Structural Basis for the Binding of Proline-Rich Peptides to SH3 Domains. *Cell.* 76:933–945.